Exploring potential astrophysical applications of black holes in nonlinear electrodynamics

Marco A. A. de Paula[1,*] and Mustapha Azreg-Aïnou[2,†]

[1]*Programa de Pós-Graduação em Física, Universidade Federal do Pará, 66075-110, Belém, Pará, Brazil*
[2]*Başkent University, Engineering Faculty, Bağlıca Campus, 06780-Ankara, Türkiye*

(Dated: October 27, 2025)

Spacetimes arising from nonlinear electrodynamics (NED) are a good laboratory for studying both the nature of regular black holes (RBH) solutions and the imprints of nonlinear electromagnetic fields within this context. Over the past few decades, NED-sourced black hole (BH) spacetimes have attracted considerable attention, but electrically charged RBHs obtained in the so-called F framework have been less addressed in the literature. We consider two members of the h-family of electrically charged, fully RBHs that are solutions to general relativity minimally coupled to NED. Because of their potential astrophysical and astronomical applications, we mainly focus our investigation on the motion of photons and its implications in the shadow radius and gravitational and kinematic redshift, considering the effective geometry followed by photons in NED. For a BH charge-to-mass ratio below some moderate value, there is almost no way to distinguish these members (and likely all members) of the h-family from the Reissner-Nordström (RN) BH. In its turn, for a BH charge-to-mass ratio above some moderate value, we observe discrepancies in their physical and geometric properties in comparison to those of the RN BH. Furthermore, we also consider observational data for Sagittarius A* and Messier 87* BHs to impose some constraints on the charge-to-mass ratio of the fully RBHs.

I. INTRODUCTION

Singularities in a space region are the place where the laws of nature break down. Such an effect is not welcomed in physics and, in general, provides an indication that the physical theory behind it has drawbacks. Singularities emerge in the theory of general relativity (GR), as they do in linear electrodynamics (LED). For example, in GR, singularities may appear as pathologies in spacetime when curvature scalars blow up [1], while, in LED, the self-energy of a point charge can be unbounded [2]. The coupling of nonlinear GR with LED has not resulted in the removal of metric and LED field singularities, even when other normal or phantom fields (scalars in general) are considered, as in Einstein-Maxwell-dilaton theory [3]. In the late 1990s, Eloy Ayón-Beato and Alberto García realized that it was possible to obtain exact charged regular black hole (RBH) solutions, i.e., black holes (BHs) free of curvature singularities, based on the minimal coupling between the GR and models of nonlinear electrodynamics (NED) [4]. This theory was originally perceived as an attempt to generalize Maxwell's theory in the ultraviolet regime [5, 6]. However, nowadays it is commonly applied in BH physics as a mathematical tool or mechanism that allows the generation of nonsingular solutions. Many investigations went in the direction of showing how this mechanism actually works [7, 8].

NED Lagrangians may either depend explicitly on the electric and/or magnetic charge, as does the Ayón-Beato and García Lagrangian [4] and the Lagrangian that produces the source for the Bardeen RBH [9, 10], or be independent of the charge [11, 12], as does the Born-Infeld Lagrangian [5]. Moreover, NED models can be represented in two related frameworks — the so-called F and P frameworks [7]. In the F framework, the field system is expressed in terms of a gauge-invariant Lagrangian $\mathcal{L}(F)$, where $F = F_{\mu\nu}F^{\mu\nu}$ is the Maxwell scalar, with $F_{\mu\nu}$ being the standard electromagnetic field tensor. The dual formalism allows us to convert the $\mathcal{L}(F)$ Lagrangian to an $\mathcal{L}(P)$ one by means of a Legendre transformation [13], leading to the P framework, where $P = P_{\mu\nu}P^{\mu\nu}$, and $P_{\mu\nu}$ is an auxiliary electromagnetic field tensor, given by $P_{\mu\nu} = \mathcal{L}_F F_{\mu\nu}$ [14]. The P framework is commonly used to obtain electrically charged RBHs.

Incorporation of NED stress-energy tensors as sources into the field equations has, in addition to smoothing the singularities, the effect of modifying the motion of photons [15]. The paths of photons are geodesics of some effective geometry (EG), $\bar{g}_{\mu\nu}$, which depends on the NED fields and is related to the background geometry, $g_{\mu\nu}$, by $\bar{g}_{\mu\nu} = \alpha_{\mu\nu} g_{\mu\nu}$ (no summation), where $\alpha_{\mu\nu}$ are functions of the NED fields [16]. Consequently, all that is related to the motion of photons in NED must take the EG into account to achieve the correct results. Over the past few years, several works have investigated the role driven by photons in NED-sourced spacetimes in the context of gravitational lensing [16–22] and thermodynamics [23–26]. Moreover, the causality condition is the requirement that the trajectories of photons are timelike in the background metric $g_{\mu\nu}$. This results in inequality constraints and theorems concerning the NED fields [27–29].

Another interesting topic — yet less explored in the context of NED-sourced spacetimes — is gravitational and kinematic redshifts. Roughly speaking, in general, a star moving in a circular orbit emits radiation that can be measured by a detector, and the redshift depends on the 4-momentum of the photon emitted by the star and received by the detector [30]. Consequently, since photons in NED propagate along null geodesics of an EG, gravitational and kinetic redshifts are expected to be affected in this scenario, as discussed, e.g., in Refs. [31, 32]. We also stress that the gravitational and kinematic redshifts are particularly significant in the environments of neutron stars, especially magnetars. Vacuum birefringence, a phenomenon associated with NED models, is expected to

* marcodepaula@ufpa.br
† azreg@baskent.edu.tr

be detectable in the neighborhood of such objects due to the strength of their magnetic field [33–35].

The static spherically symmetric (SSS) solution derived in [4], considering the P framework, has finite metric and NED fields for all values of the radial coordinate. In contrast, most known electrically charged solutions in NED minimally coupled to gravity, obtained in the F framework, have a divergent electric field at the center $r = 0$ [36]. Recently, in addition to mass and electric charge, a one-parameter family of SSS, and fully RBHs (h-family) with $-2 < h \leq 2$, where both the metric function and the electric field are regular for all values of the radial coordinate, has been determined [37]. This spacetime provides a good test ground for investigating the properties of electrically charged RBHs obtained in the F framework, as well as NED fields in this context. Here, our aim is to address the physical and geometric properties of two members of the h-family, the $h = 0$ and $h = 2$ members.

To achieve this aim, we will conduct the following investigations. In Sec. II, we introduce some preliminaries and define our working ansatzes. In Sec. III, we investigate the physical and geometric properties of the fully regular solution corresponding to $h = 0$ and $h = 2$. We elaborate on the motion of photons, considering the EG, in Sec. IV, studying the geodesic equations in IV A and the weak deflection angle in IV B. We also use observational data for Sagittarius A* (Sgr A*) and Messier 87* (M87*) BHs to impose some astrophysical constraints on the BH charge-to-mass ratio of fully RBHs in IV C. Then, because of the potential relevance of NED fields in astronomy, we elaborate on gravitational and kinematic redshifts in Sec. V. We draw our conclusions in Sec. VI. Throughout this work, we take $c = 8\pi G = 1$, and use the metric signature $(+, -, -, -)$, unless otherwise stated.

II. PRELIMINARIES

In the F framework, the field equations are derived by varying the action [7]

$$S = \frac{1}{2}\int \mathrm{d}^4x\sqrt{|g|}\,\left[R - \mathcal{L}(F)\right], \tag{1}$$

where g is the determinant of the metric tensor $\mathbf{g}$, R is the Ricci scalar, and $\mathcal{L}(F)$ represents the NED Lagragian. For convenience, we assume a general SSS metric of the form

$$\mathrm{d}s^2 = A(r)\mathrm{d}t^2 + B(r)\mathrm{d}r^2 + C(r)\mathrm{d}\Omega^2\,, \tag{2}$$

in which $A(r)$, $B(r)$, and $C(r)$ are coefficients to be determined by the field equations, and $\mathrm{d}\Omega^2 = \mathrm{d}\theta^2 + \sin^2\theta\mathrm{d}\varphi^2$ is the line element of a 2-sphere of unit radius.

The line element of an SSS metric associated with NED-sourced BH spacetimes can be written as

$$\mathrm{d}s^2 \equiv g_{\mu\nu}dx^\mu dx^\nu \tag{3}$$
$$= f(r)\mathrm{d}t^2 - f(r)^{-1}\mathrm{d}r^2 - r^2\mathrm{d}\Omega^2\,, \tag{4}$$

for which $A(r) = -B(r)^{-1} = f(r)$, with $f(r)$ being the metric function, $C(r) = -r^2$, and the field equations lead to

$$\frac{rf(r)' + f(r) - 1}{r^2} = -\frac{\mathcal{L}(F)}{2} + F\mathcal{L}_F\,, \tag{5}$$
$$\frac{rf(r)'' + 2f(r)'}{2r} = -\frac{\mathcal{L}(F)}{2}\,, \tag{6}$$

and

$$\nabla_\mu(\mathcal{L}_F\,F^{\mu\nu}) = 0\,, \tag{7}$$

where $\mathcal{L}_F = \mathrm{d}\mathcal{L}/\mathrm{d}F$ and the prime notation denotes derivative with respect to the radial coordinate r. Note that Eq. (7) is a conservation equation for the Faraday tensor, and this tensor also satisfies the Bianchi identity.

The Kretschmann scalar (KS), defined by $\mathcal{K}_\mathrm{S} \equiv R_{\mu\nu\rho\sigma}R^{\mu\nu\rho\sigma}$, related to the metric (4) has the form

$$\mathcal{K}_\mathrm{S} = \frac{4\left(1 - f(r)\right)^2 + 4r^2\left(f(r)'\right)^2 + r^4\left(f(r)''\right)^2}{r^4}\,. \tag{8}$$

It is well known that there are no regular metrics that are solutions of GR minimally coupled to LED. This could be justified as follows. In LED, Eq. (7) yields $F = -2Q^2/r^4$, and the KS reduces to

$$\mathcal{K}_\text{S-LED} = \frac{20Q^4}{r^8} - \frac{24Q^2(1 - f(r))}{r^6} + \frac{12(1 - f(r))^2}{r^4}\,, \tag{9}$$

where Q denotes the electric or magnetic charge in this case. It is clear that there is no way to make $\mathcal{K}_\text{S-LED}$ regular at the center $r = 0$ whether $f(r)$ is regular there or not. The reader may object and claim that the massless metric function $f(r) = 1 + \text{const}/r^2$ could remove the divergence at $r = 0$. First of all, we must have const $= Q^2$ but this solves only (6) and not (5). Moreover, if we assume const $\neq Q^2$ then we have to choose a complex const $= \pm\mathrm{i}(\sqrt{6}\pm 3\mathrm{i})Q^2/3$ (where $\mathrm{i}^2 = -1$) to be able to remove the singularity of $\mathcal{K}_\text{S-LED}$ at $r = 0$.

Since in this work we are interested in purely electrically charged solutions, Eq. (7) is easily integrated and yields the electric field expression $E(r)$, given by

$$E(r) = F^{tr} = \frac{Q}{r^2\mathcal{L}_F}\,, \tag{10}$$

along with that of the invariant F, namely

$$F = -2(F^{tr})^2 = -\frac{2Q^2}{r^4\mathcal{L}_F^2}\,, \tag{11}$$

with Q denoting the electric charge. In the F framework, most known electrically charged solutions in NED minimally coupled to gravity have a divergent electric field at the center $r = 0$ [36]. This singularity can be removed at the price of choosing $\mathcal{L}_F$ divergent at the center, but we can save $\mathcal{L}(F)$. There are many ways to remove the singularity at the center [37]. In this work, we choose $\mathcal{L}_F$ in the form

$$\mathcal{L}_F = \frac{1}{x^8} + \frac{h}{x^4} + 1\,, \tag{12}$$

where h is a dimensionless real parameter and x is a dimensionless radial coordinate defined in terms of r by

$$x = \frac{r}{K}\,, \tag{13}$$

in which $K = K(M,Q)$ is a positive parameter that has the dimension of length and will be given in terms of the ratio Q^2/M in the subsequent sections, with M being the Arnowitt-Deser-Misner (ADM) mass (see, e.g., Refs. [38, 39] for details). The expressions given above of F (11) and $\mathcal{L}_F$ (12) yield an expression for the product $F\mathcal{L}_{FF}$ (needed for subsequent sections), where $\mathcal{L}_{FF} = \partial_x \mathcal{L}_F/\partial_x F$, namely,

$$F\mathcal{L}_{FF} = \frac{(hx^4+2)(x^8+hx^4+1)}{x^8(x^8-hx^4-3)}\,. \tag{14}$$

As noted in [37], the electric charge of the solution is not local; rather, it is distributed spatially with a non-delta distribution function, in contrast to the Reissner Nordström (RN) solution, where the electric charge has a delta distribution.

Note that in the Maxwellian limit, we have $\mathcal{L} \to F$ (instead of $\mathcal{L} \to -F$), so that, in our case, the causality requirement that the trajectories of photons are timelike in the background metric $g_{\mu\nu}$ takes the form [11]

$$\frac{\partial^2 \mathcal{L}}{\partial E^2} \leq 0\,, \tag{15}$$

where E is the electric field defined in Eq. (10). Using $F = -2E^2$ and $\partial\mathcal{L}/\partial E = \mathcal{L}_F(\partial F/\partial E)$, we obtain

$$\frac{\partial^2 \mathcal{L}}{\partial E^2} = -4(\mathcal{L}_F + 2F\mathcal{L}_{FF}). \tag{16}$$

Considering Eq. (12), we get

$$\frac{\partial^2 \mathcal{L}}{\partial E^2} = -\frac{4(x^8+hx^4+1)^2}{x^8(x^8-hx^4-3)}\,, \tag{17}$$

which is manifestly negative if

$$r > r_{\text{CR}} \equiv K[(h+\sqrt{12+h^2})/2]^{1/4}\,, \tag{18}$$

where CR means causality requirement. Note that r_{CR} is generally smaller than the radius of the outer horizon.

III. BACKGROUNDS

In this section, we present the spacetimes that will be explored in this work, namely $h = 0$ and $h = 2$ of the h-family (see the Appendix of [37]), discussing mainly their metric function and KS. For simplicity, we define the normalized electric charge, given by

$$q \equiv \frac{Q}{Q_{\text{ext}}}, \tag{19}$$

which satisfies $0 \leq q \leq 1$ for BH solutions, where Q_{ext} is the extreme charge value of the corresponding BH solution.

A. Fully RBH spacetimes with h = 0

For $h = 0$, the NED Lagrangian that produces an asymptotically flat metric is

$$\mathcal{L}(x) = \frac{5184M^4}{\pi^4(\sqrt{2}+1)^2Q^6}\left(\frac{\pi}{2} - \frac{2x^4}{1+x^8} - \arctan x^4\right), \tag{20}$$

where x is defined in (13), with the parameter K given by

$$K := \frac{\sqrt{\sqrt{2}+1}\,\pi Q^2}{6\times 2^{1/4}M}\,. \tag{21}$$

The corresponding metric function is given by [37]

$$f(x) = 1 - \frac{36\sqrt{2}(\sqrt{2}-1)M^2}{\pi^2 Q^2}\,p(x)\,, \tag{22}$$

with

$$\begin{aligned} p(x) = \frac{1}{6x}\Big\{ & x^3(\pi - 2\arctan x^4) \\ & - \sum_{i=0}^{3}\cos(7\alpha_i)\ln\Big[1+x^2-2(\cos\alpha_i)x\Big] \\ & + 2\sum_{i=0}^{3}\sin(7\alpha_i)\arctan\Big[(\csc\alpha_i)x - \cot\alpha_i\Big]\Big\}, \end{aligned} \tag{23}$$

and

$$\alpha_i = \frac{(2i+1)\pi}{8}. \tag{24}$$

The metric function given by Eq. (22) has the following $x = 0$ and $x \to \infty$ behaviors:

$$f(r) = 1 - \frac{432\left(3-2\sqrt{2}\right)M^4}{\pi^3 Q^6}r^2 + \mathcal{O}\left[r^5\right], \tag{25}$$

$$f(r) = 1 - \frac{2M}{r} + \frac{Q^2}{r^2} - \frac{\left(17+12\sqrt{2}\right)\pi^8 Q^{18}}{181398528M^8 r^{10}} + \mathcal{O}\left[\frac{1}{r^{11}}\right], \tag{26}$$

respectively. In Fig. 1, we display the behavior of the metric function (30). We see that for $0 < q < 1$, we have RBH solutions with an event horizon r_+ and a Cauchy horizon r_-. The location of the horizons and the extreme charge value can be found by solving $f(r) = 0$ and $f'(r) = 0$ numerically. When $q = 1$, we obtain an extreme charged RBH geometry, with $r_{\text{ext}} \approx 0.9925$ and $Q_{\text{ext}} \approx 1.0009M$ being the location of the event horizon and the extreme charge value, respectively. For $q > 1$, we have horizonless solutions, whose scope is beyond this paper, and the Schwarzschild BH solution is obtained when $q = 0$. This causal structure is similar to several nonsingular charged BH geometries presented in the literature (see, e.g., Ref. [36] and references therein).

The behavior of the corresponding KS is shown in Fig. 2. We note that KS is finite in the limit $r \to 0$, namely,

$$\mathcal{K}_{\text{S}}(r) = \frac{4478976\left(17-12\sqrt{2}\right)M^8}{\pi^6 Q^{12}} + \mathcal{O}\left[r^4\right], \tag{27}$$

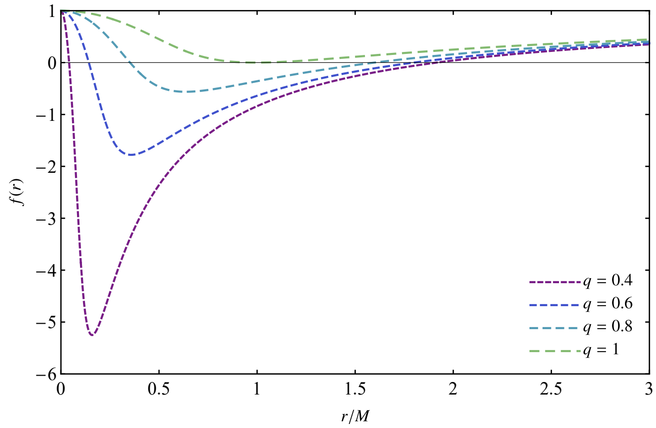

FIG. 1. Metric function (22), for distinct values of q, as a function of r/M.

which indicates that as long as $|Q|>0$, the geometry is regular for $r \geq 0$ [40, 41], in the sense that all invariants constructed from the Riemann tensor and the metric tensor are finite.

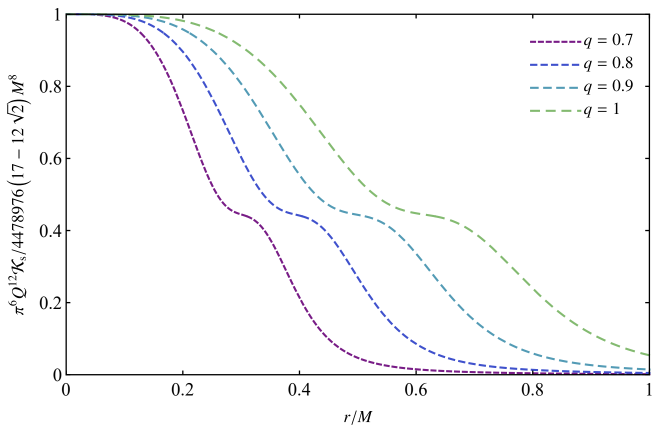

FIG. 2. KS of the spacetime given by the metric function (22), considering different choices of q, as a function of r/M.

B. Fully RBH spacetimes with h = 2

For $h=2$, the asymptotically flat metric corresponds to the following NED Lagrangian

$$\mathcal{L}(x) = \frac{2048M^4}{\pi^4 Q^6}\, \frac{1-x^4}{(1+x^4)^2}\,, \tag{28}$$

where

$$K := \frac{\pi Q^2}{4\sqrt{2}M}\,. \tag{29}$$

The metric function $f(x)$ takes the form [37]

$$f(x) = 1 - \frac{32M^2}{\pi^2 Q^2}\, p(x)\,, \tag{30}$$

and

$$p(x) = \frac{\sqrt{2}}{24x}\Big[6[\arctan(1+\sqrt{2}x) - \arctan(1-\sqrt{2}x)] + 3\ln\left(\frac{1-\sqrt{2}x+x^2}{1+\sqrt{2}x+x^2}\right)\Big]\,. \tag{31}$$

At the asymptotic limits $x=0$ and $x\to\infty$, the metric function (30) has the following behavior

$$f(r) = 1 - \frac{1024M^4}{3\pi^4 Q^6} r^2 + \mathcal{O}\left[r^3\right]\,, \tag{32}$$

$$f(r) = 1 - \frac{2M}{r} + \frac{Q^2}{r^2} - \frac{\pi^4 Q^{10}}{5120M^4 r^6} + \mathcal{O}\left[\frac{1}{r^7}\right]\,, \tag{33}$$

respectively. In Fig. 3, we show the behavior of the metric function (30). The causal structure of this spacetime is similar to that of the case given by Eq. (22), i.e., BH solutions are described by $0 \leq q \leq 1$. However, the extreme charged BH is characterized by $r_{\text{ext}} \approx 0.9526M$ and $Q_{\text{ext}} \approx 1.0108M$.

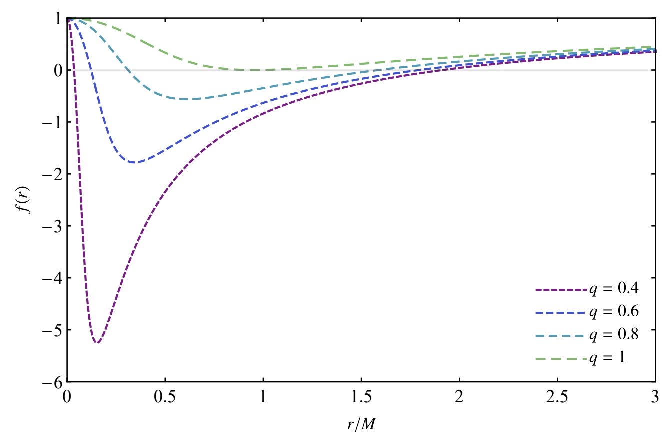

FIG. 3. Metric function (30), for distinct values of q, as a function of r/M.

The behavior of the corresponding KS is shown in Fig. 4. As we can see, the KS is finite in the limit $r\to 0$, i.e.,

$$\mathcal{K}_{\text{S}}(r) = \frac{8388608M^8}{3\pi^8 Q^{12}} + \mathcal{O}\left[r^2\right]. \tag{34}$$

Therefore, as long as $|Q|>0$, the geometry is regular.

We also point out that the de Sitter-like behavior of the metric functions (22) and (30) at their core (see Eqs. (25) and (32), respectively) is an expected feature of NED-sourced spacetimes that satisfy the weak energy condition [42]. Moreover, since the spacetimes of the h-family discussed here satisfy a correspondence with Maxwell's theory in the far-field, i.e.,

$$\mathcal{L}(F) \to F \quad \text{and} \quad \mathcal{L}_F \to 1, \tag{35}$$

for $F \ll 1$, their metric functions behave as the RN metric function for large r, which is given by

$$f^{\text{RN}}(r) \equiv 1 - \frac{2M}{r} + \frac{Q^2}{r^2}, \tag{36}$$

with higher-order corrections. For the RN spacetime, the extreme charged BH is characterized by $r_{\text{ext}} = Q_{\text{ext}} = M$.

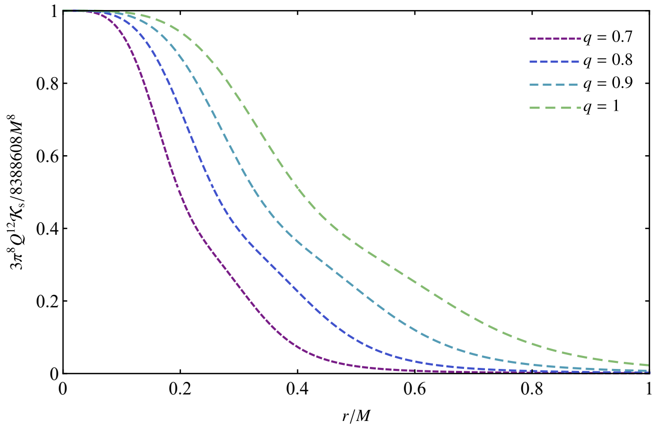

FIG. 4. KS of the spacetime given by the metric function (30), considering different choices of q, as a function of r/M.

IV. MOTION OF PHOTONS

In this section, we investigate the motion of photons in NED. Due to the spherical symmetry of the spacetime (2), we consider the motion in the equatorial plane, i.e., $\theta = \pi/2$, without loss of generality.

A. Null geodesics

As discussed in the Introduction, the motion of photons in NED is not described by the standard geometry (SG), rather by the EG [15]. The EG metric can be written as [7]

$$\bar{g}^{\mu\nu} = \mathcal{L}_F g^{\mu\nu} - 4\mathcal{L}_{FF} F^{\mu}{}_{\alpha} F^{\alpha\nu}\,, \tag{37}$$

and the corresponding line element results in

$$\begin{aligned} \mathrm{d}\bar{s}^2 &\equiv \bar{g}_{\mu\nu} dx^{\mu} dx^{\nu} && (38)\\ &= \frac{1}{\Phi}\left(f(r)\mathrm{d}t^2 - \frac{1}{f(r)}\mathrm{d}r^2\right) - \frac{r^2}{\mathcal{L}_F}\,\mathrm{d}\Omega^2\,, && (39)\end{aligned}$$

where $\Phi = \mathcal{L}_F + 2F\mathcal{L}_{FF}$. For LED, we have $\bar{g}^{\mu\nu} = g^{\mu\nu}$.

Following the same approach presented in Refs. [16, 29], we apply the Hamiltonian formalism in curved spacetimes to analyze the geodesic motion. The Hamiltonian that provides the equations of motion for photons in the EG is given by

$$\begin{aligned} H &\equiv \frac{1}{2}\bar{g}^{\mu\nu}\bar{p}_{\mu}\bar{p}_{\nu},\\ &= \frac{1}{2}\left[\Phi\left(\frac{\bar{p}_t^2}{f(r)} - f(r)\,\bar{p}_r^2\right) - \frac{\mathcal{L}_F \bar{p}_{\varphi}^2}{r^2}\right], \end{aligned} \tag{40}$$

where $\bar{p}_{\mu}$ (p_{μ}) are the components of the four-momentum of photons (massless particles). Since $\bar{p}_{\mu} = \bar{g}_{\mu\nu}\dot{x}^{\nu}$, we find

$$\dot{t} = \frac{\Phi E_{\text{ph}}}{f(r)}, \tag{41}$$

$$\dot{r} = -f(r)\Phi\bar{p}_r, \tag{42}$$

$$\dot{\varphi} = \frac{\mathcal{L}_F L_{\text{ph}}}{r^2}, \tag{43}$$

for which the overdot stands for differentiation with respect to an affine parameter. Due to the symmetries of the Hamiltonian (40) on the coordinates t and φ, we take $\bar{p}_t \equiv E_{\text{ph}}$ and $\bar{p}_{\varphi} \equiv -L_{\text{ph}}$ as constants of motion, where E_{ph} and L_{ph} are the energy and angular momentum of photons, respectively. To avoid misinterpretation, we have added the subscript "ph" to the energy and angular momentum of the photon.

Using Eqs. (40)-(43), and $H = 0$, we find that

$$\left(\frac{\dot{r}}{\Phi}\right)^2 + V(r) = E_{\text{ph}}^2, \tag{44}$$

where $V(r)$ is defined as

$$V(r) \equiv L_{\text{ph}}^2 \frac{\mathcal{L}_F f(r)}{\Phi r^2}. \tag{45}$$

Closed circular photon orbits are described by $\dot{r} = 0$ and $\ddot{r} = 0$, which implies that $V(r) = E^2$ and $V'(r) = 0$, respectively. Moreover, if $V''(r) < 0$, then the closed circular-photon orbit is unstable. From $\dot{r} = 0$, we obtain the critical impact parameter associated with the light ring (LR), namely

$$b_l = r_l \sqrt{\frac{\Phi_l}{(\mathcal{L}_F)_l\, f_l}}, \tag{46}$$

where $f(r_l) \equiv f_l$ and r_l is the radial coordinate of the closed circular photon orbit. Moreover, from $\ddot{r} = 0$, we obtain the corresponding radial coordinate of the LR, given by

$$f_l\left[2 - \frac{r_l\left((\mathcal{L}_F)_l\right)'}{(\mathcal{L}_F)_l} + \frac{r_l\left(\Phi_l\right)'}{\Phi_l}\right] - r_l f_l' = 0, \tag{47}$$

where the subscript "l" denotes that the quantity under consideration is computed at the radial coordinate of the LR r_l. If the NED model satisfies a correspondence with Maxwell's theory, see the conditions given by Eqs. (35), Eqs. (44)-(47) reduce to the corresponding results for massless particles [43].

In this case, $\mathcal{L}_F \to 1$ and $\Phi \to 1$, and instead of the LR coordinate, we have a critical radius r_c associated with the critical impact parameter b_c. In LED, these results describe the motion of photons, but in NED, they describe the motion of massless particles with a nature other than electromagnetic.

We note that concerning the perspective of static observers in NED-sourced spacetimes, the NED fields introduce non-trivial contributions to the motion of photons. Consequently, for an observer placed at an arbitrary location outside the event horizon, the critical impact parameter will not necessarily correspond to the shadow radius [16]. To properly analyze this problem, we can investigate the orbit equation (44).

Using Eqs. (43) and (44), we can show that

$$\frac{dr}{d\varphi} = \pm r\sqrt{\frac{f(r)\Phi}{\mathcal{L}_F}\left[\frac{r^2\Phi E_{\text{ph}}^2}{f(r)\mathcal{L}_F L_{\text{ph}}^2} - 1\right]}. \tag{48}$$

Moreover, the turning point, R, of the photon orbit, i.e., the radius of the nearest point, is given by

$$\left.\frac{dr}{d\varphi}\right|_{r=R} = 0. \tag{49}$$

Combining Eqs. (48) and (49), we can find an expression for $E_{\rm ph}/L_{\rm ph}$ at the turning point R and rewrite Eq. (48) as

$$\frac{dr}{d\varphi} = \pm r\sqrt{\frac{f(r)\Phi}{\mathcal{L}_F}\left[\frac{r^2\Phi f_R \mathcal{L}_F(R)}{R^2\Phi_R f(r)\mathcal{L}_F} - 1\right]}. \qquad (50)$$

If we consider a static observer placed at $r_{\rm o}$ sending a light ray that is transmitted into the past with an angle β with respect to the radial direction, we obtain

$$\cot\beta = \frac{\bar{g}_{rr}}{\bar{g}_{\varphi\varphi}}\sqrt{\frac{g_{\varphi\varphi}}{g_{rr}}}\frac{dr}{d\varphi}\bigg|_{r=r_{\rm o}} = \frac{\mathcal{L}_F}{r f(r)^{1/2}\Phi}\frac{dr}{d\varphi}\bigg|_{r=r_{\rm o}}. \qquad (51)$$

The corresponding expression of Eq. (51) in LED was derived in [44]. Injecting Eq. (50) into Eq. (51), and using $\sin^2\beta = 1/(1+\cot^2\beta)$, we find that the shadow radius of electrically charged NED-sourced BHs is given by

$$\bar{r}_s = r_{\rm o}\sin\beta = r_{\rm o} b_l \sqrt{\frac{f_{\rm o}\Phi_{\rm o}}{r_{\rm o}^2\Phi_{\rm o} + b_l^2 f_{\rm o}\left(\Phi_{\rm o} - \mathcal{L}_F(r_{\rm o})\right)}}, \qquad (52)$$

where b_l is given in (46) in terms of r_l, which is the radius of the photon sphere solution to Eq. (47). We point out that $\Phi_{\rm o} - \mathcal{L}_F(r_{\rm o})$ in Eq. (52) can be negative for $h=0$ if

$$r < r_{\rm eff}^{h=0} \equiv \frac{\sqrt{1+\sqrt{2}}\pi Q^2}{2\sqrt[4]{2}3^{7/8}M}, \qquad (53)$$

where $r_{\rm eff}$ is an effective radius, and for the case $h=2$, if

$$r < r_{\rm eff}^{h=2} \equiv \frac{\sqrt[4]{3}\pi Q^2}{4\sqrt{2}M}. \qquad (54)$$

However, one can show that $r_{\rm eff}^{h=0}$ and $r_{\rm eff}^{h=2}$ are typically located within the BH, i.e., $r_+ > r_{\rm sig}$. Therefore, we conclude that the shadow radius is not affected by this behavior.

Notice also that if we place the static observer very far away from the BH, i.e., for $r_{\rm o}\to\infty$, we have

$$\bar{r}_s = b_l, \qquad (55)$$

as expected for static and spherically symmetric spacetimes. We emphasize that the result presented by Eq. (55) works for fully RBHs with $h=0$ and $h=2$, but may not be valid for arbitrary NED sourced spacetimes. Moreover, we denote the "shadow radius" computed according to the SG as r_s.

The ratio between the shadow radius, considering the effective and standard geometries, can help us quantify how much the EG affects the shadow shape compared to the SG. For $h=2$, as shown in Fig. 5, we see that $\bar{r}_{\rm s}$ is typically greater than $r_{\rm s}$. The greatest difference between them occurs for the extreme charged case, where $\bar{r}_{\rm s}\approx 1.01346 r_{\rm s}$. Moreover, the comparison with the RN case shows that the shadow radius of the RBH with $h=2$ is smaller (greater) than that of the RN case for $q < q_{\rm crit} \cong 0.971611$ ($q > q_{\rm crit}$).

The results for $h=0$ on the ratio between the shadow radius computed considering the standard and effective geometries are qualitatively similar to those of the case $h=2$. The highest difference occurs for the extreme charged case, for which $\bar{r}_{\rm s}\approx 1.00284 r_{\rm s}$. Nevertheless, compared to the RN case, the results for $h=0$ are different from those obtained for the case $h=2$. As shown in Fig. 6, for the case $h=0$, the corresponding shadow radius is typically smaller than that for the RN case regardless of the value of q.

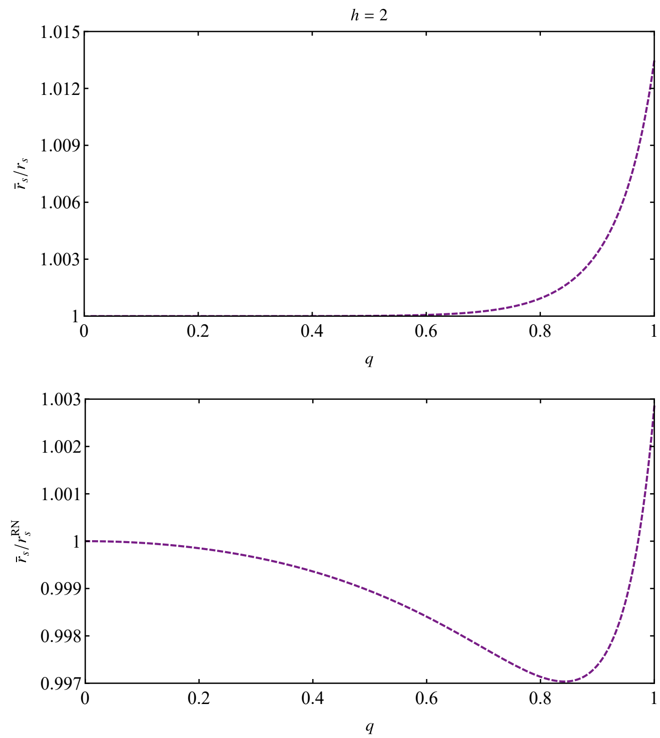

FIG. 5. Ratio between the shadow radius of the fully RBH with $h=2$, as a function of q, for two distinct scenarios: (i) considering the effective $\bar{r}_{\rm s}$ and standard $r_{\rm s}$ geometries (top panel); and (ii) considering $\bar{r}_{\rm s}$ and the shadow radius of the RN case, denoted by $r_{\rm s}^{\rm RN}$ (bottom panel).

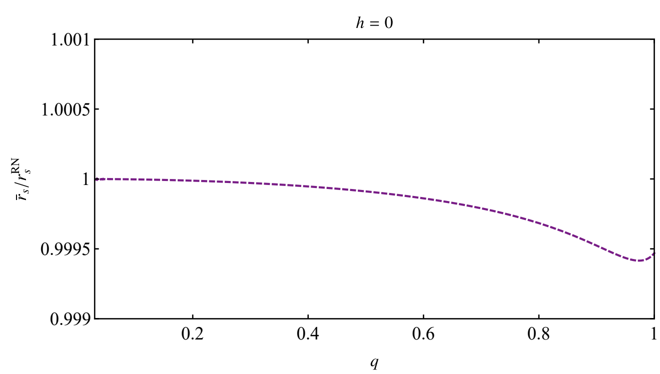

FIG. 6. Ratio between the shadow radius of the fully RBH with $h=0$, as a function of q, considering $\bar{r}_{\rm s}$ and the shadow radius of the RN case $r_{\rm s}^{\rm RN}$.

Therefore, for fully RBH solutions with $h=0$ or $h=2$ [37], the difference between the shadow radius considering the standard and effective geometries is very small. This result is in contrast to those obtained for other NED-sourced BH geometries [16]. Despite the similarity, the EG is still necessary to calculate the proper motion of photons [28, 29, 45].

B. Weak deflection angle

Here, we use the Gauss-Bonnet theorem [46] (see, e.g., Refs. [47–51], and references therein for more details) to derive an expression for the weak deflection angle of the $h = 0$ and $h = 2$ family of fully RBH solutions in the weak field limit, considering the standard and effective geometries.

The line element of the optical metric related to the motion of massless particles can be obtained by setting $\mathrm{d}s^2 = 0$ and $\theta = \pi/2$ in the line element (4). Thus, we get

$$dt^2 = h_{\mu\nu}dx^\mu dx^\nu = dr_\star^2 + v(r_\star)^2 d\varphi^2. \tag{56}$$

where $r_\star$ is the Regge–Wheeler coordinate, defined by $dr_\star = f(r)^{-1}dr$, and $v(r_\star) \equiv r/\sqrt{f(r)}$. The corresponding Ricci scalar R associated with this geometry is given by

$$R = -\frac{2}{v(r_\star)}\frac{d^2 v(r_\star)}{dr_\star^2}, \tag{57}$$

and the Gaussian optical curvature $\mathcal{K}$ yields $\mathcal{K} = R/2$.

The Gauss-Bonnet theorem allows us to relate the deflection angle $\Theta(b)$ to the Gaussian optical curvature $\mathcal{K}$ through a simple equation, given by [46]

$$\Theta(b) = -\int_0^{\pi+\alpha}\int_{u(\varphi)}^{\infty}\mathcal{K}\mathrm{d}S, \tag{58}$$

where

$$\mathrm{d}S = \sqrt{|h|}\mathrm{d}r_\star \mathrm{d}\varphi, \tag{59}$$

with h being the determinant of the metric tensor $h_{\mu\nu}$. The parameters α and $u(\varphi)$ are corrections in the observer's position and the trajectory of the particle, respectively. They can be obtained by solving the radial orbit equation. For the general SSS metric given by Eq. (2), we have

$$\frac{du}{d\varphi} + u^4 C(r)\left(\frac{1}{A(r)B(r)b^2} + \frac{1}{C(r)B(r)}\right) = 0, \tag{60}$$

where we defined $r \equiv 1/u$, with $u = u(\varphi)$.

For our purposes, we can set the correction as $\alpha = 4M/b$, and suppose that $u(\varphi)$ is given by

$$u(\varphi) = \frac{1}{b}\left[u_0(\varphi) + \frac{M}{b}u_1(\varphi) + \frac{M^2}{b^2}u_2(\varphi)\right], \tag{61}$$

where the coefficients $u_k(\varphi)$, with $k = 1$, 2, or 3, can be obtained using an iterative method [52]. For fully RBH solutions with $h = 0$ and $h = 2$, the corresponding coefficients result in the same expressions since both exhibit Maxwell-like behavior in the far field. By inserting Eq. (61) into Eq. (60), we obtain the following differential equation for $u_0(\varphi)$:

$$\left(\frac{du_0}{d\varphi}\right)^2 + u_0^2 - 1 = 0, \tag{62}$$

for which the physical solution is given by

$$u_0(\varphi) = \sin\varphi. \tag{63}$$

For $u_1(\varphi)$, we find that

$$\cot\varphi\left(\frac{du_1}{d\varphi}\right) + u_1 - \sin^2\varphi = 0, \tag{64}$$

and the corresponding solution yields

$$u_1(\varphi) = (1-\cos\varphi)^2. \tag{65}$$

Finally, for $u_2(\varphi)$, we get

$$M^2\left[\cos\varphi\frac{du_2}{d\varphi} + \sin\varphi u_2\right] + \sin^4\left(\frac{\varphi}{2}\right)\left[4(Q^2-M^2)\cos\varphi + (3M^2+Q^2)\cos 2\varphi + M^2 + 3Q^2\right] = 0, \tag{66}$$

and this yields

$$u_2(\varphi) = \frac{6\varphi\left(Q^2-5M^2\right)\cos\varphi + \sin\varphi\left(-\left(3M^2+Q^2\right)\cos(2\varphi) + 32M^2\cos\varphi + M^2 - 5Q^2\right)}{8M^2}. \tag{67}$$

The corresponding expression for $u(\varphi)$ is obtained by inserting Eqs. (63), (65), and (67) into Eq. (61). We note that the equations for $u(\varphi)$, as well as the expansion $\mathcal{K}dS$ up to the fourth order in r, are the same for the cases $h = 0$ and $h = 2$. Therefore, one can show that the weak deflection angle of the standard and effective metrics, considering Eq. (22) or Eq. (30), coincide up to the third order in $1/b^3$, leading to

$$\Theta(b) = \frac{4M}{b} + \frac{3\pi\left(5M^2-Q^2\right)}{4b^2} + \frac{16M\left(8M^2-3Q^2\right)}{3b^3} + \mathcal{O}\left[\frac{1}{b^4}\right], \tag{68}$$

which coincides with the RN result [53], and for $Q = 0$ we obtain the Schwarzschild result. The similarity to the RN case can be understood by noting that the charge contributions associated with the fully RBHs discussed in this work are proportional to $1/r^{10}$, see the metric function given by Eq. (26), and to $1/r^6$, see the metric function given by Eq. (33). Consequently, the charge contributions are very small at the weak-field limit. To search for perturbations arising from the fully RBHs in the weak deflection angle, considering the standard and effective geometries, we need to consider more correction orders, which is beyond the scope of this work.

C. Astrophysical constraints

In this section, we aim to impose astrophysical constraints in the BH charge-to-mass ratio Q/M of the fully RBH solutions with $h = 0$ and $h = 2$ using observational data for Sgr A* and M87*. The bounds in the shadow radius of Sgr A* [54] and M87* [55] consistent with the most updated observations for the constraints 1σ and 2σ are resumed in Tab. I. For Sgr A*, we consider the data of the instruments/teams Keck [56] and the Very Large Telescope Interferometer (VLTI) [57], while for M87*, we consider the data from the Event Horizon Telescope (EHT) collaboration [58].

BHs	Constraints	
	1σ	2σ
Sgr A*	$4.55 \lesssim r_s/M \lesssim 5.22$	$4.21 \lesssim r_s/M \lesssim 5.56$
M87*	$4.26 \lesssim r_s/M \lesssim 6.03$	$3.38 \lesssim r_s/M \lesssim 6.91$

TABLE I. Bounds in the shadow radius of Sgr A* and M87*.

In Fig. 7, we compare our results for the shadow radius of case $h = 2$ with the Keck/VLTI observational data for Sgr A*. We note that the data set the 1σ upper limits $Q \lesssim 0.7999M$ and $Q \lesssim 0.79979M$, considering the effective and standard geometries, respectively. On the other hand, the 2σ constraints lead to the upper limits $Q \lesssim 0.9466M$ and $Q \lesssim 0.9392M$, considering the standard and effective geometries, respectively. Therefore, observational data rule out the possibility that Sgr A* is an extremely charged fully RBH with $h = 2$, as occurs for the RN case, up to 2σ constraints. Yet, moderately charged fully RBHs with $h = 2$ are still feasible.

In Fig. 8, we compare our results for the shadow radius of the case $h = 2$ with the EHT observational data for M87*. We note that the EHT observations for M87* set the 1σ upper limits $Q \lesssim 0.9282M$ and $Q \lesssim 0.9219M$ for the effective and standard geometries, respectively. On the other hand, the results for $Q \leq Q_{\text{ext}}$ are consistent with the 2σ constraints. Consequently, the EHT observations show that M87* is consistent with extremely charged fully RBH solutions with $h = 2$ for 2σ constraints, but, when considering 1σ constraints, only for at most moderately charged fully RBHs with $h = 2$.

The bounds for the charge-to-mass ratio for the case $h = 0$ are very similar to those of the case $h = 2$. Consequently, the conclusions are basically the same. To illustrate this, in Tab. II, we resume the main results for the $h = 0$ case.

It is also interesting to verify how large the charge-to-mass ratio Q/M is in physical units, considering the EG, and to compare it to some bounds obtained from astrophysical considerations. To do this, we first restore the physical units. Consider $Q = \rho M$, where ρ is a numerical value. In physical units, $M \to GM/c^2$ and $Q^2 \to GQ^2/4\pi\epsilon_0 c^4$, where G is the gravitational constant, c is the speed of light, and ϵ_0 is

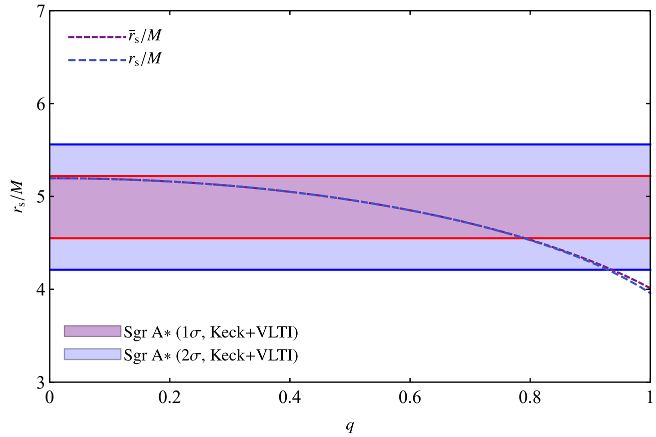

FIG. 7. Shadows radius of fully RBHs with $h = 2$, considering the standard and effective geometries, as a function of q. The light blue and purple regions are consistent with the EHT horizon-scale image of Sgr A* at 1σ and 2σ constraints, respectively. The white regions denote the excluded regions.

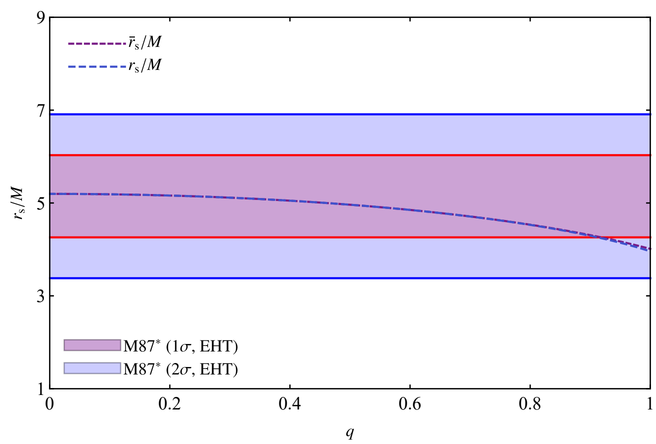

FIG. 8. Shadows radius of fully RBHs with $h = 2$, considering the standard and effective geometries, as a function of q. The light blue and purple regions are consistent with the EHT horizon-scale image of M87* at 1σ and 2σ constraints, respectively. The white regions denote the excluded regions.

BHs	Sgr A*		M87*	
Constraints	1σ	2σ	1σ	2σ
$(Q/M)^{\text{SG}}$	0.797959	0.938977	0.921972	–
$(Q/M)^{\text{EG}}$	0.797963	0.936068	0.928275	–

TABLE II. Bounds to the charge-to-mass ratio of fully RBHs with $h = 0$, considering the standard and effective geometries and the observational data for Sgr A* and M87*. The symbol "–" denotes that the BHs for $h = 0$ are within the range of the data constraints, regardless the value of Q/M.

the vacuum permittivity. Therefore, we have

$$Q = 2M\rho\sqrt{G\pi\epsilon_0}. \tag{69}$$

As the results for $h = 0$ are similar to those of $h = 2$, we consider the values of the ratio Q/M for case $h = 2$. In this case, for constraints 1σ and 2σ, considering Sgr A*, we have $Q \approx 5.41716 \times 10^{26}C$ and $Q \approx 6.41065 \times 10^{26}C$, respectively, where we use $M_{\text{Sgr}A^\star} = 3,951 \times 10^6 M_\odot$ [56]. Concerning M87*, we have $Q \approx 1.03421 \times 10^{30}C$ and $Q \approx 1.12621 \times 10^{30}C$, where we use $M_{\text{M87}^\star} = 6,5 \times 10^9 M_\odot$ [59], for the constraints 1σ and 2σ, respectively.

The results for the charge-to-mass ratio obtained using the data for Sgr A* can be compared with the charge constraints of Sgr A* obtained in Refs. [60, 61]. The extreme charge of Sgr A* is $Q^{\text{ext}}_{\text{Sgr}A^\star} \approx 4 \times 10^{27}$ [62]. However, in astrophysical scenarios, the charge of Sgr A* is expected to have the upper limits $Q \lesssim 3 \times 10^8 C$ [60] or $Q \lesssim 3 \times 10^{15} C$ [61], depending on the astrophysical setup. Therefore, our results for fully RBH solutions with $h = 0$ and $h = 2$ show that their charges are close to the extremely charged case of Sgr A*, but remarkably larger than the upper limits on the Sgr A* charge.

V. GRAVITATIONAL AND KINEMATIC REDSHIFTS

A. Main equations

We assume the presence of a star orbiting a NED RBH given by a general metric of the form given by Eq. (2), with $A(r) = g_{tt}(r)$, $B(r) = g_{rr}(r)$, and $C(r) = g_{\varphi\varphi}(r)$[1]. The star emits radiation, the frequency of which is measured by a detector (usually at spatial infinity). We aim to determine the maximum and minimum values of the redshift (we use the term redshift to mean either redshift or blueshift). In LED, such expressions are known in the literature in the case where $g_{\varphi\varphi}(r) = r^2$ [63], considering the metric signature $(-,+,+,+)$ and $\theta = \pi/2$. We will derive the most general expression of the redshift that applies to NED too. While we are using an SSS metric with signature $(+,-,-,-)$, we will provide an expression for the redshift and intermediate expression that are valid for both SSS-metric signatures $(+,-,-,-)$ and $(-,+,+,+)$. We introduce the symbol ϵ, given by $\epsilon = +1$, if the metric signature is $(+,-,-,-)$, and $\epsilon = -1$, if the metric signature is $(-,+,+,+)$. We have $\epsilon g_{tt} = |g_{tt}|$ and $-\epsilon g_{\varphi\varphi} = |g_{\varphi\varphi}|$.

The star, emitting radiation, is supposed to move in a circular orbit in the plane $\theta = \pi/2$ with 4-velocity $u^\mu = (u^t, 0, 0, u^\varphi)$. Circular motion is treated in many references and we can show that the specific energy E and the angular momentum L of the star, treated as a particle following a circular geodesic, are given by

$$E^2 = \frac{|g_{tt}|\,(\ln|g_{\varphi\varphi}|)'}{(\ln|g_{\varphi\varphi}|)' - (\ln|g_{tt}|)'}\,, \tag{70}$$

$$L^2 = \frac{|g_{\varphi\varphi}|\,(\ln|g_{tt}|)'}{(\ln|g_{\varphi\varphi}|)' - (\ln|g_{tt}|)'}\,, \tag{71}$$

they satisfy, respectively, the conservation equations:

$$E = \epsilon g_{tt} u^t = |g_{tt}| u^t\,, \quad L = -\epsilon g_{\varphi\varphi} u^\varphi = |g_{\varphi\varphi}| u^\varphi\,. \tag{72}$$

If k^μ is the 4-momentum of the photon emitted by the star, the frequency of the emitted photon is $\omega_e = \epsilon g_{\mu\nu} k^\mu_e u^\nu$, where $u^\mu = (u^t, 0, 0, u^\varphi)$ is the 4-velocity of the star and k^μ_e is the value of k^μ at the star position. The frequency of the photon absorbed (received) by the detector is $\omega_d = \epsilon g_{\mu\nu}(\infty) k^\mu_d U^\nu$, where $U^\mu = (1/\sqrt{|g_{tt}(\infty)|}, 0, 0, 0)$ is the 4-velocity of the detector and $k^\mu_d = k^\mu(\infty)$. The extreme values of the redshift are obtained when the photon ray, in the plane $\theta = \pi/2$, is tangent to the circle, i.e., when $k^\mu = (k^t, 0, 0, k^\varphi)$. Using (72), we obtain that the frequencies are given by

$$\omega_e = E k^t_e - L k^\varphi_e\,, \qquad \omega_d = k^t_d \sqrt{|g_{tt}(\infty)|}\,. \tag{73}$$

The redshift z is defined by $z \equiv (\lambda_d - \lambda_e)/\lambda_e$ [64], where (λ_e, λ_d) are the corresponding wavelengths. In terms of (ω_e, ω_d), the redshift can be written as

$$z = \frac{\omega_e}{\omega_d} - 1 = \frac{k^t_e}{k^t_d\sqrt{|g_{tt}(\infty)|}}\Big(E - L\frac{k^\varphi_e}{k^t_e}\Big) - 1\,, \tag{74}$$

where E and L are given by Eqs. (70) and (71), respectively. To evaluate k^φ_e/k^t_e we use the fact that the photon 4-momentum satisfies the constraint $\bar{g}_{\mu\nu} k^\mu k^\nu = 0$, which yields

$$\frac{k^\varphi_e}{k^t_e} = \pm\sqrt{\frac{|\bar{g}_{tt}|}{|\bar{g}_{\varphi\varphi}|}}\,. \tag{75}$$

Without loss of generality, we can always choose $L > 0$. With this choice at hand, the "+" sign corresponds to $k^\varphi_e > 0$, which means that at the moment of emission the star was approaching the detector and this yields a minimum value for z, $z_{\text{min}} = z_+$. The "$-$" sign corresponds to $k^\varphi_e < 0$, the star was receding at the moment of emission, yielding a maximum value for z, $z_{\text{max}} = z_-$. Now, the EG $\bar{g}_{\mu\nu}$ (37) is of the form $\bar{g}_{\mu\nu} = \alpha_{\mu\nu} g_{\mu\nu}$ [no summation and $\text{sgn}(\bar{g}_{\mu\nu}) = \text{sgn}(g_{\mu\nu})$], where $\alpha_{\mu\nu}$ are scalar (positive) functions of coordinates given in terms of the NED fields. This reduces the expressions of $z_\pm$ to

$$z_\pm = \frac{k^t_e}{k^t_d\sqrt{|g_{tt}(\infty)|}}\left(E \mp L\sqrt{\frac{\alpha_{tt}|g_{tt}|}{\alpha_{\varphi\varphi}|g_{\varphi\varphi}|}}\right) - 1\,, \tag{76}$$

where the upper (lower) sign on the left-hand side corresponds to the upper (lower) sign on the right-hand side. The photon obeys conservation equations similar to Eq. (72) but in the EG, where its path is a geodesic, we have $\bar{E}_{\text{ph}} = \epsilon \bar{g}_{tt} k^t =$

[1] In what follows, we assume the motion in the equatorial plane, thus $r^2 d\Omega^2 \to r^2 d\varphi^2$. Therefore, for simplicity, we label $C(r) = g_{\varphi\varphi}(r)$.

$|\bar{g}_{tt}|k^t$ [compare with (41) where the constants $\bar{E}_{\text{ph}}$ and E_{ph} are proportional]. This yields $|\bar{g}_{tt}|k_e^t = |\bar{g}_{tt}(\infty)|k_d^t$, that is

$$\frac{k_e^t}{k_d^t} = \frac{|\bar{g}_{tt}(\infty)|}{|\bar{g}_{tt}|} = \frac{\alpha_{tt}(\infty)|g_{tt}(\infty)|}{\alpha_{tt}|g_{tt}|}\,, \tag{77}$$

and

$$z_\pm = \frac{\alpha_{tt}(\infty)\sqrt{|g_{tt}(\infty)|}}{\alpha_{tt}|g_{tt}|}\left(E \mp L\sqrt{\frac{\alpha_{tt}|g_{tt}|}{\alpha_{\varphi\varphi}|g_{\varphi\varphi}|}}\right) - 1\,. \tag{78}$$

Finally, substituting the expressions for E and L, given by Eqs. (70)-(71), we obtain the general expression of the redshift for an SSS metric in the presence of a NED field, namely

$$z_\pm = \frac{\alpha_{tt}(\infty)\sqrt{|g_{tt}(\infty)|}}{\alpha_{tt}\sqrt{|g_{tt}|}\sqrt{(\ln|g_{\varphi\varphi}|)' - (\ln|g_{tt}|)'}}\times \left(\sqrt{(\ln|g_{\varphi\varphi}|)'} \mp \sqrt{(\ln|g_{tt}|)'}\sqrt{\frac{\alpha_{tt}}{\alpha_{\varphi\varphi}}}\right) - 1\,, \tag{79}$$

where $z_{\text{min}} = z_+$ and $z_{\text{max}} = z_-$. In LED, the functions $\alpha_{\mu\nu}$ are all unity. In our case, as previously noticed, $\alpha_{tt}(\infty) = 1$ and $|g_{tt}(\infty)| = 1$ because Eq. (37) is asymptotically flat.

Upon applying Eq. (79) to our case under investigation, with $\alpha_{tt} = 1/\Phi$, $\alpha_{\varphi\varphi} = 1/\mathcal{L}_F$ and $|g_{tt}| = f(r)$ (30) and $|g_{\varphi\varphi}| = r^2$, we obtain,

$$z_\pm = \frac{\Phi}{\sqrt{f}\sqrt{1 - \frac{rf'}{2f}}}\left(1 \mp \sqrt{\frac{rf'}{2f}}\sqrt{\frac{\mathcal{L}_F}{\Phi}}\right) - 1\,. \tag{80}$$

If the star were not moving ($u^\varphi = 0$ and $L = 0$), see Eq. (72), we would obtain the purely gravitational redshift. The star 4-velocity would be $u^\mu = (1/\sqrt{|g_{tt}|}, 0, 0, 0)$, the emitted frequency $\omega_e = k_e^t\sqrt{|g_{tt}|}$, and

$$z_{\text{grav}} = \frac{k_e^t\sqrt{|g_{tt}|}}{k_d^t\sqrt{|g_{tt}(\infty)|}} - 1\,, \tag{81}$$

where k_e^t/k_d^t is still given by Eq. (77). Finally,

$$z_{\text{grav}} = \frac{\alpha_{tt}(\infty)}{\alpha_{tt}}\sqrt{\frac{g_{tt}(\infty)}{g_{tt}}} - 1\,. \tag{82}$$

The kinematic redshift (Doppler part), i.e., $z_{\pm(\text{kin})} = z_\pm - z_{\text{grav}}$, can be written as

$$z_{\pm(\text{kin})} = \frac{\alpha_{tt}(\infty)}{\alpha_{tt}}\sqrt{\frac{g_{tt}(\infty)}{g_{tt}}}\times \left[\frac{\sqrt{(\ln|g_{\varphi\varphi}|)'} \mp \sqrt{(\ln|g_{tt}|)'}\sqrt{\frac{\alpha_{tt}}{\alpha_{\varphi\varphi}}}}{\sqrt{(\ln|g_{\varphi\varphi}|)' - (\ln|g_{tt}|)'}} - 1\right]\,. \tag{83}$$

This is the general expression for the kinematic redshift. For our case, we obtain

$$z_{\pm(\text{kin})} = \frac{\Phi}{\sqrt{f}}\left[\frac{1 \mp \sqrt{\frac{rf'}{2f}}\sqrt{\frac{\mathcal{L}_F}{\Phi}}}{\sqrt{1 - \frac{rf'}{2f}}} - 1\right]\,. \tag{84}$$

B. Results for $h = 0$ and $h = 2$ cases

It is the kinematic redshift that is measured by astronomers. In Fig. 9, we plot the kinematic redshifts $z_{\text{max (kin)}}$ and $z_{\text{min (kin)}}$ for the NED metric (30) and in Fig. 10, we plot the difference between the kinematic redshifts for the NED metric (30) and the corresponding entities for the RN BH. The second plots show that the maximum (redshift) or minimum (blueshift) kinematic redshift for the NED metric (30) is greater than that for the RN BH. This difference is more pronounced in the vicinity of the smallest circular geodesic defined by $2f - rf' = 0$.

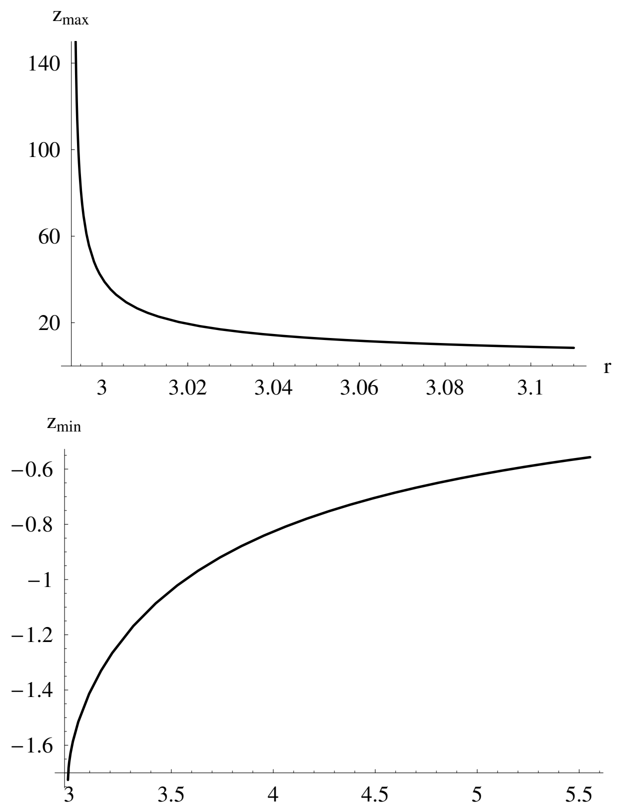

FIG. 9. Plots of the kinematic redshifts $z_{\text{max (kin)}}$ and $z_{\text{min (kin)}}$ for the NED metric (30). We took $M = 1$ and $Q = 0.1$.

Despite the difference between the NED metrics (22) and (30), their kinematic redshifts for $M = 1$, $Q = 0.1$ are almost identical. In Table III we provide values for $z_{\text{max (kin)}}$ and $z_{\text{min (kin)}}$ for both metrics for different values of the radial coordinate r when $M = 1$, $Q = 0.1$. Note that the corresponding values of $x(= r/K)$ are different due to the different values of K in (29) and in (21) for a given set of M, Q values. For these values $M = 1$, $Q = 0.1$, x is relatively large [$r = 2.998 \leftrightarrow x = 438.231$ (22) and $r = 2.998 \leftrightarrow x = 539.83$ (30)] and this explains why the kinematic redshifts are almost equal and equal to the corresponding values of the RN BH.

We can have a better idea if we go through numerical estimations. For the average value $\lambda_e = 545$ nm of the visible color spectrum (from 380 nm to 710 nm) and $r = 3.0M$, we

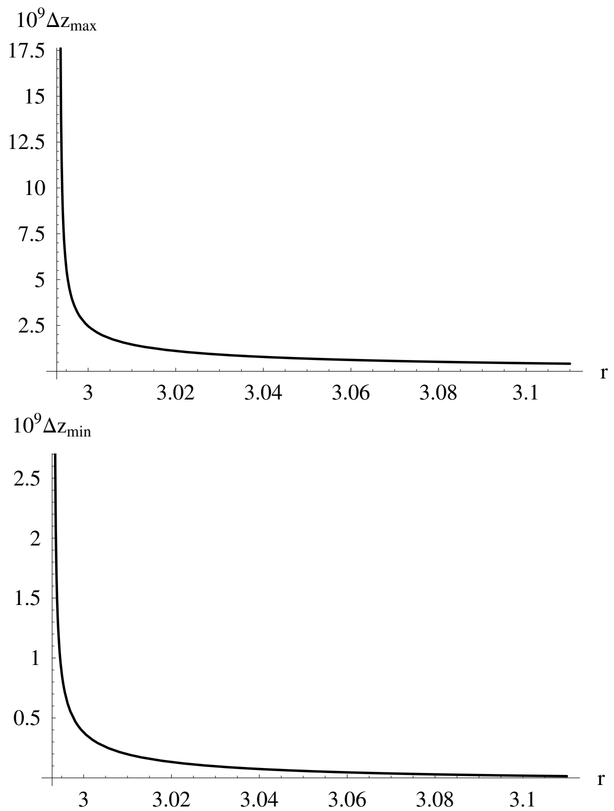

FIG. 10. Plots of differences of kinematic redshifts times 10^9: $10^9\Delta z_{\max}$ and $10^9\Delta z_{\min}$ where $\Delta z_{\max} = z_{\max\,(\text{kin})} - z_{\max\,(\text{kin-RN})}$ and $\Delta z_{\min} = z_{\min\,(\text{kin})} - z_{\min\,(\text{kin-RN})}$ with $z_{\max\,(\text{kin})}$ and $z_{\min\,(\text{kin})}$ being the kinematic redshifts related to the NED metric (30) and $z_{\max\,(\text{kin-RN})}$ and $z_{\min\,(\text{kin-RN})}$ being the kinematic redshifts for the RN BH. We took $M = 1$ and $Q = 0.1$.

r	$z_{\min\,(\text{kin})}$ (22)	$z_{\min\,(\text{kin})}$ (30)	$z_{\max\,(\text{kin})}$ (22)	$z_{\max\,(\text{kin})}$ (30)
2.998	−1.67116	−1.67116	48.8787	48.8787
3.010	−1.61259	−1.61259	25.061	25.061
3.110	−1.3937	−1.3937	8.38739	8.38739
3.200	−1.27739	−1.27739	5.8935	5.8935
5.100	−0.608431	−0.608431	1.15783	1.15783

TABLE III. Values of $z_{\max\,(\text{kin})}$ and $z_{\min\,(\text{kin})}$ corresponding to the NED metrics (22) and (30). We took $M = 1,\ Q = 0.1$.

obtain, using the kinematic redshift expression (84), $\lambda_{d\,(\max)} - \lambda_{d\,(\max\,\text{RN})} = 1.34496 \times 10^{-6}$ nm, which might be difficult to measure. However, if the light emitted passes adjacent to the smallest circular geodesic defined by $2f - rf' = 0$, where $r \simeq 2.99338M$ (not very different from $r = 3.0M$), we obtain, for the same average value λ_e, $\lambda_{d\,(\max)} - \lambda_{d\,(\max\,\text{RN})} = 7.71665 \times 10^{-5}$ nm, which represents more than 57 times the previous value.

For much larger values of Q/M, say $M = 1,\ Q = 0.79$, x is on the order of r [$r = 2.998 \leftrightarrow x = 7.0218$ (22) and $r = 2.998 \leftrightarrow x = 8.64973$ (30)] and the kinematic redshifts tend to diverge, as shown in Table IV.

For stars orbiting in the vicinity of the smallest circular geodesic, defined by $2f - rf' = 0$, it is much easier to distinguish, using the kinematic redshift, NED metrics from each other and from the RN BH in the case of a moderate ratio $Q/M \gtrsim 0.79$.

r	$z_{\min\,(\text{kin})}$ (22)	$z_{\min\,(\text{kin})}$ (30)	$z_{\max\,(\text{kin})}$ (22)	$z_{\max\,(\text{kin})}$ (30)
2.501	−1.81576	−1.37687	351.068	1217.44
2.511	−1.72411	−1.71552	33.3172	33.5357
2.998	−1.06611	−1.0665	3.29278	3.29574
3.110	−1.00014	−1.00049	2.85167	2.85384
5.100	−0.552904	−0.552942	0.986436	0.986531

TABLE IV. Values of $z_{\max\,(\text{kin})}$ and $z_{\min\,(\text{kin})}$ corresponding to the NED metrics (22) and (30). We took $M = 1,\ Q = 0.79$.

As we can see from Eqs. (26) and (33), the effect of including the NED fields was almost just to remove the singularity at the center $r = 0$, without greatly modifying the physical and geometric properties of the RN BH. This character is also observed in the kinematic redshift, where, for instance, *at least* the first eight terms of the power expansion of $z_{+(\text{kin})}$ are identical to those of the minimum kinematic redshift of the RN BH, i.e.,

$$z_{+(\text{kin-RN})} = -\sqrt{\frac{M}{r}} + \frac{1}{2}\frac{M}{r} + a_{\frac{3}{2}}\left(\frac{M}{r}\right)^{\frac{3}{2}} + \cdots + a_4\left(\frac{M}{r}\right)^4. \tag{85}$$

The six coefficients $a_{\frac{3}{2}}$, a_2, $a_{\frac{5}{2}} \ \to\ a_4$ are functions of Q^2/M^2 (for example, $a_{3/2} = [(Q^2/M^2) - 5]/2)$. Notice that the first term, $\sqrt{M/r}$, is v/c in the classical mechanics approximation.

VI. FINAL REMARKS

NED-sourced spacetimes are interesting testing grounds for investigating the properties of RBHs and also the imprints of very strong electromagnetic fields in compact object physics. This is supported by two perspectives. First, NED provides a medicine to cure curvature singularities, making a rich class of RBH solutions feasible. Second, photons in NED follow null geodesics according to an effective light cone. To broaden our knowledge on these topics, we have addressed the physical and geometrical properties of a recent family of electrically charged RBHs — the so-called h-family [37]. In particular, we explored the motion of photons, considering the EG, by investigating the shadow radius, the weak deflection angle, and the gravitational and kinematic redshifts.

Considering the shadow radius, we have derived the correct formula for a static observer, placed at a given radial position, that is sending a light ray to the past with an angle β with respect to the radial direction. Our findings show that for the h-family of BHs studied here, the EG does not deeply affect the shadow radius. We also imposed some astrophysical constraints on the BH ratio Q/M based on observational data. In particular, we have shown that the BH charges in SI units are close to the extremely charged case of Sgr A*, but substantially higher than the upper limits on the Sgr A* charge.

One of our priority in this work was to determine the total redshift expression (79) that applies to any spherically symmetric metric in the presence of NED fields. Since astronomers usually measure the kinematic redshift (Doppler effect), we had to determine its general maximum and minimum expressions (83). Applying these expressions to two NED metrics members of the h-family, we have observed amplification of the kinematic redshift when the emitting star moves in the vicinity of the smallest circular geodesic provided $Q/M \gtrsim 0.79$. This effect allows us not only to distinguish between the NED metrics and the RN BH, but also to fix one of the NED-solution parameters if the two others are known a priori, suggesting a potential astrophysical relevance.

We have noticed that for moderate and higher values of the electric charge, there are notable discrepancies between the physical and geometric behaviors of the NED metrics and the RN BH. This includes the shadow of the BH solution and the kinematic redshift. For the weak deflection angle, however, the results are very similar up to the $1/b^3$ approximation due to the far-field behavior of the NED metrics.

Possible avenues for this work are discussed as follows. In general, nonlinear electromagnetic fields are expected to play a major role in the strong-field regime. Therefore, it would be interesting to investigate the deflection angle in the strong field limit [65–67], with the aim of capturing possible effects associated with NED fields. Moreover, throughout this paper, we have considered NED models that depend solely on F. For an NED structure depending on the two electromagnetic scalars, we may have birefringence [15]. In this case, light rays can follow different paths according to their polarization. This opens up the possibility of investigating the relationship between this phenomenon and the gravitational and kinematic redshift. Furthermore, our results were restricted to the BH case, but it is known that the NED framework can be used to obtain other compact objects, such as wormholes [68, 69], which also makes studies in this vein worthwhile. Finally, in real astrophysical scenarios, BHs are expected to spin. Consequently, a further extension of the results presented in this work is to consider rotating geometries sourced by NED models.

ACKNOWLEDGMENTS

M.P. thanks the Federal University of Pará.

[1] R. M. Wald, *General relativity*. University of Chicago Press, Chicago, United States, 1984.
[2] R. Feynman, R. Leighton, and M. Sands, *The Feynman Lectures on Physics, Vol. II: The New Millennium Edition: Mainly Electromagnetism and Matter*. The Feynman Lectures on Physics, Basic Books, 2011.
[3] G. Clément, J. C. Fabris, and M. E. Rodrigues, “Phantom black holes in Einstein-Maxwell-dilaton theory,” *Phys. Rev. D*, vol. 79, no. 6, p. 064021, 2009.
[4] E. Ayón-Beato and A. García, “Regular black hole in general relativity coupled to nonlinear electrodynamics,” *Phys. Rev. Lett.*, vol. 80, pp. 5056–5059, 1998.
[5] M. Born and L. Infeld, “Foundations of the new field theory,” *Proceedings of the Royal Society of London. Series A, Containing Papers of a Mathematical and Physical Character*, vol. 144, no. 852, pp. 425–451, 1934.
[6] M. Born, “On the quantum theory of the electromagnetic field,” *Proceedings of the Royal Society of London. Series A, Containing Papers of a Mathematical and Physical Character*, vol. 143, no. 849, pp. 410–437, 1934.
[7] K. A. Bronnikov, “Regular magnetic black holes and monopoles from nonlinear electrodynamics,” *Phys. Rev. D*, vol. 63, p. 044005, 2001.
[8] S. V. Bolokhov, K. A. , and M. V. Skvortsova, “A Regular Center Instead of a Black Bounce,” *Gravit. Cosmol.*, vol. 30, p. 265, 2024.
[9] J. Bardeen, “Non-singular general relativistic gravitational collapse,” in *Proceedings of the 5th International Conference on Gravitation and the Theory of Relativity*, p. 87, 1968.
[10] E. Ayon-Beato and A. Garcia, “The Bardeen model as a nonlinear magnetic monopole,” *Phys. Lett. B*, vol. 493, pp. 149–152, 2000.
[11] D. P. Sorokin, “Introductory Notes on Non-linear Electrodynamics and its Applications,” *Fortsch. Phys.*, vol. 70, no. 7-8, p. 2200092, 2022.
[12] K. A. Bronnikov, “Regular black holes as an alternative to black bounce,” *Phys. Rev. D*, vol. 110, p. 024021, 2024.
[13] S. A. Gutierrez, A. L. Dudley, and J. F. Plebanski, “Signals and Discontinuities in General Relativistic Nonlinear Electrodynamics,” *J. Math. Phys.*, vol. 22, pp. 2835–2848, 1981.
[14] L. Balart and E. C. Vagenas, “Regular black hole metrics and the weak energy condition,” *Phys. Lett. B*, vol. 730, pp. 14–17, 2014.
[15] M. Novello, V. A. De Lorenci, J. M. Salim, and R. Klippert, “Geometrical aspects of light propagation in nonlinear electrodynamics,” *Phys. Rev. D*, vol. 61, p. 045001, 2000.
[16] M. A. A. de Paula, H. C. D. Lima Junior, P. V. P. Cunha, and L. C. B. Crispino, “Electrically charged regular black holes in nonlinear electrodynamics: Light rings, shadows, and gravitational lensing,” *Phys. Rev. D*, vol. 108, no. 8, p. 084029, 2023.
[17] Z. Stuchlík and J. Schee, “Shadow of the regular Bardeen black holes and comparison of the motion of photons and neutrinos,” *Eur. Phys. J. C*, vol. 79, no. 1, p. 44, 2019.
[18] A. S. Habibina and H. S. Ramadhan, “Geodesic of nonlinear electrodynamics and stable photon orbits,” *Phys. Rev. D*, vol. 101, no. 12, p. 124036, 2020.
[19] B. Toshmatov, B. Ahmedov, and D. Malafarina, “Can a light ray distinguish charge of a black hole in nonlinear electrodynamics?,” *Phys. Rev. D*, vol. 103, no. 2, p. 024026, 2021.
[20] A. Allahyari, M. Khodadi, S. Vagnozzi, and D. F. Mota, “Magnetically charged black holes from non-linear electrodynamics and the Event Horizon Telescope,” *J. Cosmol. Astropart. Phys.*, vol. 02, p. 003, 2020.
[21] Z. Hu, Z. Zhong, P.-C. Li, M. Guo, and B. Chen, “QED effect on a black hole shadow,” *Phys. Rev. D*, vol. 103, no. 4, p. 044057, 2021.
[22] E. F. Eiroa, “Gravitational lensing by Einstein-Born-Infeld black holes,” *Phys. Rev. D*, vol. 73, p. 043002, 2006.

[23] L. Balart and S. Fernando, "A Smarr formula for charged black holes in nonlinear electrodynamics," *Mod. Phys. Lett. A*, vol. 32, no. 39, p. 1750219, 2017.
[24] Y. Abe, M. Médevielle, T. Noumi, and K. Yoshimura, "Causality Constraints on Black Hole Thermodynamics in Nonlinear Electrodynamics," 2025, 2505.23483.
[25] E. Aydiner, E. Sucu, and I. Sakallı, "Regular Magnetically Charged Black Holes from Nonlinear Electrodynamics: Thermodynamics, Light Deflection, and Orbital Dynamics," 2025, 2507.05145.
[26] A. Bokulić, T. Jurić, and I. Smolić, "Black hole thermodynamics in the presence of nonlinear electromagnetic fields," *Phys. Rev. D*, vol. 103, no. 12, p. 124059, 2021.
[27] G. O. Schellstede, V. Perlick, and C. Lämmerzahl, "On causality in nonlinear vacuum electrodynamics of the Plebański class," *Annalen Phys.*, vol. 528, no. 9-10, pp. 738–749, 2016.
[28] J. G. Russo and P. K. Townsend, "Causal self-dual electrodynamics," *Phys. Rev. D*, vol. 109, no. 10, p. 105023, 2024.
[29] M. A. A. de Paula, H. C. D. Lima, Junior., P. V. P. Cunha, C. A. R. Herdeiro, and L. C. B. Crispino, "Good tachyons, bad bradyons: Role reversal in Einstein-nonlinear-electrodynamics models," *Phys. Lett. B*, vol. 866, p. 139513, 2025.
[30] M. P. Hobson, G. P. Efstathiou, and A. N. Lasenby, *General relativity: an introduction for physicists*. Cambridge University Press, 2006.
[31] H. J. Mosquera Cuesta and J. M. Salim, "Nonlinear electrodynamics and the gravitational redshift of pulsars," *Mon. Not. Roy. Astron. Soc.*, vol. 354, pp. L55–L59, 2004.
[32] E. Guzman-Herrera and N. Breton, "Light propagation in the vicinity of the ModMax black hole," *JCAP*, vol. 01, p. 041, 2024.
[33] R. P. Mignani, V. Testa, D. G. Caniulef, R. Taverna, R. Turolla, S. Zane, and K. Wu, "Evidence for vacuum birefringence from the first optical-polarimetry measurement of the isolated neutron star RX J1856.5−3754," *Mon. Not. Roy. Astron. Soc.*, vol. 465, no. 1, pp. 492–500, 2017.
[34] L. M. Capparelli, A. Damiano, L. Maiani, and A. D. Polosa, "A note on polarized light from Magnetars," *Eur. Phys. J. C*, vol. 77, no. 11, p. 754, 2017.
[35] J. Adam *et al.*, "Measurement of e^+e^- Momentum and Angular Distributions from Linearly Polarized Photon Collisions," *Phys. Rev. Lett.*, vol. 127, no. 5, p. 052302, 2021.
[36] K. A. Bronnikov, *in Regular Black Holes–Towards a New Paradigm of Gravitational Collapse, Ed. C. Bambi*. Springer Nature Singapore, 2023, arXiv:2211.00743v1 [gr-qc].
[37] M. Azreg-Aïnou, "Two-sided NED black-hole, naked-singularity, and soliton solutions," *Eur. Phys. J. C*, vol. 85, no. 6, p. 711, 2025.
[38] Z.-Y. Fan and X. Wang, "Construction of Regular Black Holes in General Relativity," *Phys. Rev. D*, vol. 94, no. 12, p. 124027, 2016.
[39] B. Toshmatov, Z. Stuchlík, and B. Ahmedov, "Comment on "Construction of regular black holes in general relativity"," *Phys. Rev. D*, vol. 98, no. 2, p. 028501, 2018.
[40] F. S. N. Lobo, M. E. Rodrigues, M. V. de Sousa Silva, A. Simpson, and M. Visser, "Novel black-bounce spacetimes: wormholes, regularity, energy conditions, and causal structure," *Phys. Rev. D*, vol. 103, no. 8, p. 084052, 2021.
[41] K. A. Bronnikov and S. G. Rubin, *Black Holes, Cosmology and Extra Dimensions*. World Scientific Publishing Company, Singapore, 2012.
[42] I. Dymnikova, "Regular electrically charged structures in nonlinear electrodynamics coupled to general relativity," *Class. Quant. Grav.*, vol. 21, pp. 4417–4429, 2004.
[43] M. A. A. Paula, L. C. S. Leite, and L. C. B. Crispino, "Electrically charged black holes in linear and nonlinear electrodynamics: Geodesic analysis and scalar absorption," *Phys. Rev. D*, vol. 102, no. 10, p. 104033, 2020.
[44] A. Belhaj, L. Chakhchi, H. El Moumni, J. Khalloufi, and K. Masmar, "Thermal Image and Phase Transitions of Charged AdS Black Holes using Shadow Analysis," *Int. J. Mod. Phys. A*, vol. 35, no. 27, p. 2050170, 2020.
[45] S. Murk and I. Soranidis, "Light rings and causality for nonsingular ultracompact objects sourced by nonlinear electrodynamics," *Phys. Rev. D*, vol. 110, no. 4, p. 044064, 2024.
[46] G. W. Gibbons and M. C. Werner, "Applications of the Gauss-Bonnet theorem to gravitational lensing," *Class. Quant. Grav.*, vol. 25, p. 235009, 2008.
[47] A. Övgün, "Weak field deflection angle by regular black holes with cosmic strings using the Gauss-Bonnet theorem," *Phys. Rev. D*, vol. 99, no. 10, p. 104075, 2019.
[48] W. Javed, J. Abbas, and A. Övgün, "Deflection angle of photon from magnetized black hole and effect of nonlinear electrodynamics," *Eur. Phys. J. C*, vol. 79, no. 8, p. 694, 2019.
[49] W. Javed, A. Hamza, and A. Övgün, "Effect of nonlinear electrodynamics on the weak field deflection angle by a black hole," *Phys. Rev. D*, vol. 101, no. 10, p. 103521, 2020.
[50] Q.-M. Fu, L. Zhao, and Y.-X. Liu, "Weak deflection angle by electrically and magnetically charged black holes from nonlinear electrodynamics," *Phys. Rev. D*, vol. 104, no. 2, p. 024033, 2021.
[51] M. Okyay and A. Övgün, "Nonlinear electrodynamics effects on the black hole shadow, deflection angle, quasinormal modes and greybody factors," *JCAP*, vol. 01, no. 01, p. 009, 2022.
[52] H. Arakida and M. Kasai, "Effect of the cosmological constant on the bending of light and the cosmological lens equation," *Phys. Rev. D*, vol. 85, p. 023006, 2012.
[53] C. R. Keeton and A. O. Petters, "Formalism for testing theories of gravity using lensing by compact objects. I. Static, spherically symmetric case," *Phys. Rev. D*, vol. 72, p. 104006, 2005.
[54] S. Vagnozzi *et al.*, "Horizon-scale tests of gravity theories and fundamental physics from the Event Horizon Telescope image of Sagittarius A," *Class. Quant. Grav.*, vol. 40, no. 16, p. 165007, 2023.
[55] L. Chakhchi, H. El Moumni, and K. Masmar, "Signatures of the accelerating black holes with a cosmological constant from the Sgr A$\star$ and M87$\star$ shadow prospects," *Phys. Dark Univ.*, vol. 44, p. 101501, 2024.
[56] T. Do *et al.*, "Relativistic redshift of the star S0-2 orbiting the Galactic center supermassive black hole," *Science*, vol. 365, no. 6454, pp. 664–668, 2019.
[57] R. Abuter *et al.*, "Detection of the Schwarzschild precession in the orbit of the star S2 near the Galactic centre massive black hole," *Astron. Astrophys.*, vol. 636, p. L5, 2020.
[58] K. Akiyama *et al.*, "First M87 Event Horizon Telescope Results. I. The Shadow of the Supermassive Black Hole," *Astrophys. J. Lett.*, vol. 875, p. L1, 2019.
[59] K. Akiyama *et al.*, "First M87 Event Horizon Telescope Results. VI. The Shadow and Mass of the Central Black Hole," *Astrophys. J. Lett.*, vol. 875, no. 1, p. L6, 2019.
[60] M. Zajaček, A. Tursunov, A. Eckart, S. Britzen, E. Hackmann, V. Karas, Z. Stuchlík, B. Czerny, and J. A. Zensus, "Constraining the charge of the Galactic centre black hole," *J. Phys. Conf. Ser.*, vol. 1258, no. 1, p. 012031, 2019.
[61] M. Zajaček, A. Tursunov, A. Eckart, and S. Britzen, "On the charge of the Galactic centre black hole," *Mon. Not. Roy. Astron. Soc.*, vol. 480, no. 4, pp. 4408–4423, 2018.
[62] L. Iorio, "Constraining the electric charges of some astronomi-

cal bodies in Reissner-Nordstrom spacetimes and generic r^{-2}-type power-law potentials from orbital motions," *Gen. Rel. Grav.*, vol. 44, pp. 1753–1767, 2012.

[63] K. Lake, "Galactic potentials," *Phys. Rev. Lett.*, vol. 92, p. 051101, 2004.

[64] B. Schutz, *A first course in general relativity*. Cambridge university press, 2022.

[65] V. Bozza, "Gravitational lensing in the strong field limit," *Phys. Rev. D*, vol. 66, p. 103001, 2002.

[66] E. F. Eiroa and C. M. Sendra, "Gravitational lensing by a regular black hole," *Class. Quant. Grav.*, vol. 28, p. 085008, 2011.

[67] N. Tsukamoto, "Deflection angle in the strong deflection limit in a general asymptotically flat, static, spherically symmetric spacetime," *Phys. Rev. D*, vol. 95, no. 6, p. 064035, 2017.

[68] K. A. Bronnikov, "Nonlinear electrodynamics, regular black holes and wormholes," *Int. J. Mod. Phys. D*, vol. 27, no. 06, p. 1841005, 2018.

[69] K. A. Bronnikov and R. K. Walia, "Field sources for Simpson-Visser spacetimes," *Phys. Rev. D*, vol. 105, no. 4, p. 044039, 2022.